

# Interaction between laser radiation and a plasma corona at flux densities $10^{14}$ – $10^{15}$ W/cm<sup>2</sup>

Yu. A. Zakharenkov, N. N. Zorev, O. N. Krokhin, Yu. A. Mikhailov, A. A. Rupasov, G. V. Sklizkov, and A. S. Shikanov

*P. N. Lebedev Physics Institute, USSR Academy of Sciences, Moscow*  
(Submitted August 11, 1975)  
*Zh. Eksp. Teor. Fiz.* 70, 547–559 (February 1976)

Results are reported of experimental studies of the interaction between laser radiation and plasma produced by heating flat targets by light fluxes of  $10^{14}$ – $10^{15}$  W/cm<sup>2</sup>. Specially developed composite techniques (ultrahigh-speed interferometry at  $2\omega_0$ , multichannel x-ray pinhole cameras, probing with a laser beam of different wavelength) have been used to obtain new data on the parameters of the corona. The density profile has been established between  $10^{18}$  and  $2.4 \times 10^{21}$  cm<sup>-3</sup> (the critical density for  $\lambda_0 = 1.06 \mu$  is  $10^{21}$  cm<sup>-3</sup>). The evolution of the density profile is accompanied by the appearance of perturbations (cavitons). A singularity in the region of the critical density has been found. The formation of jets has been recorded in the hot part of the plasma. Results are given of detailed investigations of the scattered and reflected light at frequencies of  $\omega_0$  and  $2\omega_0$ , showing the presence of a shift in the position of the second-harmonic line maximum in the direction of longer wavelengths. The evolution in time of the width of the generation region at  $2\omega_0$  has been measured. Hard x rays with energies  $\geq 150$  keV have been recorded.

PACS numbers: 52.25.Ps

Laser-controlled thermonuclear fusion is a new topic in thermonuclear physics, currently undergoing rapid development. The success achieved so far, for example, the detection of a considerable number of neutrons<sup>[1]</sup> produced in the laser plasma, the experimental demonstration of a strong compression of material at the center of an isolated spherical target,<sup>[1,2]</sup> and a reduction down to  $10^4$ – $10^5$  J in the theoretical value of the laser energy necessary for a physically convenient thermonuclear reaction,<sup>[3]</sup> have focused increased attention on the question of the interaction between high-intensity laser radiation and plasma.<sup>[4]</sup>

Although the energy that can be generated by modern laser systems is still substantially lower than that necessary for a physically convenient thermonuclear reaction, the rates of energy release and the laser flux densities which are already available do correspond to those that will be used in laser-controlled thermonuclear systems. This means that the simulation and investigation of processes occurring in the corona of a target used in such systems can be investigated now or in the immediate future.

We report in this paper a continuation of our previous experiments<sup>[5–8]</sup> designed to elucidate the processes involved in the interaction between high-intensity light and plasma. In contrast to previous studies in which the density profile could be followed up to  $5 \times 10^{19}$  cm<sup>-3</sup>, in the present work we used special composite methods of measurement (interferometry, x rays, harmonics, and laser-beam probing) to establish the profile between  $10^{18}$  and  $2.4 \times 10^{21}$  cm<sup>-3</sup> (the critical density for  $\lambda_0 = 1.06 \mu$  is  $10^{21}$  cm<sup>-3</sup>). We have found a singularity in the critical region in the form of a caviton-type perturbation of the profile of the corona, and the formation of jets in the hot part of the corona recorded by x-ray pinhole cameras. We also report the results of measurements on the scattered and reflected radiation at  $\omega_0$  and  $2\omega_0$ .

## 1. EXPERIMENTAL ARRANGEMENT

Plasma heating was achieved with the aid of a nine-channel neodymium-glass laser system.<sup>[9]</sup> This system is illustrated in Fig. 1 together with the diagnostic equipment. The pulse from the neodymium-glass laser (1) was truncated by the Kerr cell (2) which was controlled by the laser-fired discharge gap (3). To improve contrast, the radiation was allowed to pass twice through the shaping Kerr cell. The light pulse emerg-

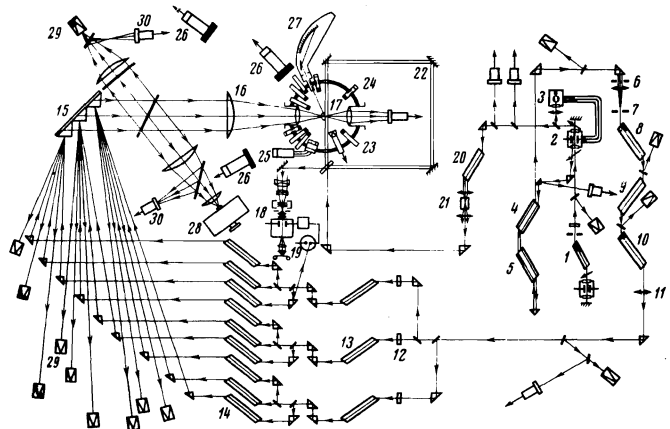


FIG. 1. Schematic arrangement of the apparatus: 1—neodymium-glass laser using a Kerr cell Q switch; 2—Kerr cell shaper; 3—laser-fired discharge gap; 4, 5—double-pass amplifying stages; 6—long focal length lens; 7—slit; 8–10—final stages of the preamplifier; 11—lens; 12—transparent filters; 13, 14—high-power amplifying stages; 15—nine-prism reflector; 16—focusing system; 17—vacuum chamber; 18—photorecorder; 19—laser-fired discharge gap controlling the photorecorder; 20—amplifier; 21—KDP crystal; 22—interferometer; 23—multichannel film detectors; 24—multichannel pinhole cameras; 25—multichannel detection of hard x rays; 26—neutron detectors; 27—x-ray spectrograph; 28—MDR-2 monochromator (VMS-1 and ISP-51 spectrographs not shown); 29—calorimeters; 30—coaxial photocells.

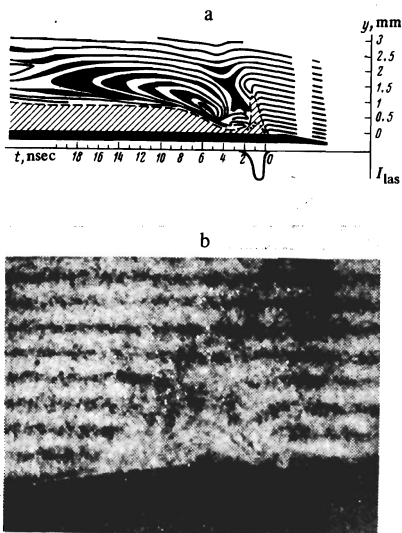


FIG. 2. (a) Slit scan of the interferogram due to a laser flare (the slit of the photorecorder is perpendicular to the target surface); the hatched area shows the opacity zone. (b) Frame interferogram of laser plasma at time  $t = 1.5$  nsec after the arrival of the heating pulse. Width of interference band  $160 \mu$ .

ing from this cell was amplified by the two-stage system (4, 5), in which the radiation passed twice through each rod.

Next, the radiation was focused by the long focal length lens (6), and subsequent amplification in the three stages (8, 9, 10) of the preamplifier system was carried out in a divergent beam. The slit (7) at the focus of the lens protected the preamplifier and pulse-shaping system from the effect of radiation reflected from plasma and amplified in the various stages of the generating system.

A special lens (11), which collimated the beam and corrected the astigmatism produced at optical surfaces at the Brewster angle, was placed at the exit from the preamplifying system. The radiation was then allowed to enter the high-power amplification system (HPA).<sup>[10]</sup> The radiation amplified by the HPA system<sup>[13,14]</sup> was collected into a single beam with a diameter of about 18 cm by the nine-prism reflector (15) and the two-component lens (16), and was focused on the surface of a flat target at the center of the vacuum chamber (17). The laser energy in the present series of experiments was up to 200–250 J for a pulse length  $\tau \approx 1$  nsec, beam divergence  $\alpha \approx 3 \times 10^{-4}$  rad, and contrast  $\sim 10^6$ . Because of imperfections in the focusing system, the flux density averaged over the pulse length and over the focal spot was up to about  $5 \times 10^{14}$  W/cm<sup>2</sup>. To reduce the coupling between the target and the laser, the angle between the normal to the plane of the target and the laser beam was chosen to be about  $13^\circ$ . Moreover, a number of passive shutters (12) with initial transmission of about 10% was introduced into the system. The targets were solid specimens and thin films of ordinary (CH<sub>2</sub>)<sub>n</sub> and deuterized (CD<sub>2</sub>)<sub>n</sub> polyethylene, and aluminum.

The plasma was investigated by the following methods: (1) high-speed interferometry both with slit scanning of the image on an electron-optical converter and frame-

by-frame photography, (2) detection of continuous x rays in the band between 1 and 10 Å, using x-ray sensitive photographic film, (3) measurements on soft x rays emitted by the plasma, using spatial resolution (multi-channel pinhole camera), (4) measurements on plasma emission at the harmonic frequency of the heating radiation with both spatial and temporal resolution, and (5) measurements of the spectral composition of the radiation incident on and reflected by the plasma. In addition, we used special detectors to record neutrons and hard x rays ( $h\nu \geq 100$  keV), and the x-ray spectrograph (27) for the band between 10 and 1000 Å, but the results obtained by these techniques will not be reviewed here.

We begin by considering the main techniques listed above.

### High-speed interferometry

Interferometry with a time resolution better than  $10^{-10}$  sec, using the electron-optical converter (18), was found to be more successful under the conditions of slit scanning. The operation of the photodetector system was synchronized with the process under investigation with the aid of the laser-controlled discharge gap (19)<sup>[11]</sup> which had a dead time of less than 1 nsec. When the system was operated under slit scanning conditions, the interferometer was illuminated as follows. A pulse of radiation from the neodymium-glass laser, having a length of about 20–30 nsec at half-power points, was extracted through the polished side face of a Glan prism in the pulse-shaping Kerr cell. The light pulse was then amplified by the amplifier (20) and was converted by the KDP crystal (21) into the second harmonic ( $\lambda = 5300$  Å) of the neodymium-laser frequency. The interferogram (see Fig. 2a) was recorded in the light of this second-harmonic radiation.

The design of the interferometer (22) (four-mirror shearing interferometer with opposite ray paths)<sup>[11]</sup> was capable, depending on the particular requirements, of combining the advantages of the Mach-Zender, Jamin, and differential interferometers.<sup>[12]</sup> We note that, in the last interferometers, a comparison is made between the phases of coherent light waves transmitted by an inhomogeneity with a small lateral shift. Among the advantages of such systems is the fact that it is possible to vary the sensitivity to density gradients, which is very important in inhomogeneous laser-plasma diagnostics. Another important fact is that the interferometer which we have used automatically ensures equal optical path lengths for the two interfering rays, which means that, in principle, the interference pattern can be recorded in white light.

In addition to slit scanning, frame-by-frame photography of the interferograms was carried out for each pulse (Fig. 2b). In this case, the interferometer is illuminated by part of the heating pulse which was transformed by a second KDP crystal (not shown in Fig. 1) into radiation of wavelength  $0.53 \mu$  and pulse length  $\sim 1$  nsec.

The fringe shift function obtained experimentally was approximated on a computer by a set of Chebyshev

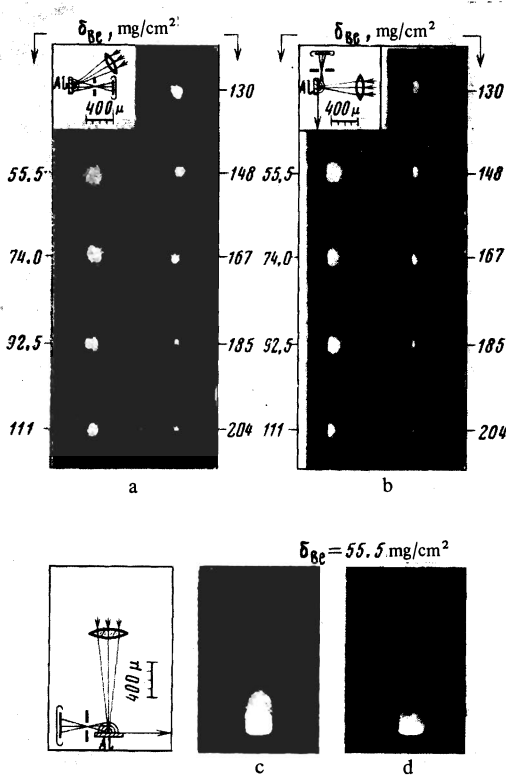


FIG. 3. (a), (b) Typical eighteen-frame pinhole camera photograph of laser plasma for two directions of observation. (c) Image of plasma elongated in the direction of the laser beam. (d) Appearance of individual jets. Spatial resolution in all cases  $20 \mu$ .

polynomials, using a least-squares procedure. The resulting function was substituted into the Abel integral, and the radial distribution of electron density in plasma was determined analytically.<sup>[13]</sup> The optimum order of the approximating polynomial was determined with the aid of a statistical test of significance and the conditional probability for the polynomial. Test calculations in which the exact distribution  $N_e(r)$  was known demonstrated the high accuracy and stability of the solution. It is important to note, however, that when the Abel integral is used, it is essential to take into account the symmetry properties of the inhomogeneity under investigation, and a correct analysis of interference patterns is possible only in the plane perpendicular to the axis of symmetry. In the case of laser plasma and sharply focused radiation on the surface of a flat target, the most important density profile is that along the heating beam, i.e., along the axis of symmetry. This means that additional data on the shape of surfaces of equal electron density are necessary in the analysis of interferograms obtained by slit scattering when the EOC slit is perpendicular to the target image. This can be obtained from interferograms obtained by frame photography and, independently, from the analysis of photographs obtained with the x-ray pinhole cameras (see below). It was found that the shape of these equal-density surfaces could be satisfactorily approximated by a family of ellipses with constant eccentricity and common point on the surface of the target. If we denote

the ratio of semiaxes by  $k$ , we find that the shift of an interference band is given by

$$\delta(y) = 4.46 \cdot 10^{-14} \lambda k \int_y^R \frac{N_e(r) y^{1/2} dr}{(r-y)^{3/2}}$$

where  $y$  is measured along the axis of symmetry,  $R$  is the radius of the plasma, and  $r$  is the distance along the axis of the ellipse perpendicular to the target. The solution of this integral equation can also be obtained with the aid of the Abel transformation:

$$N_e(r) = -\frac{1}{4.46 \cdot 10^{-14} \lambda \pi k} \int_r^R \left( \frac{\delta(y)}{y^{1/2}} \right)' \frac{dy}{(y-r)^{1/2}}$$

We note that, when the isodensity surfaces are approximated by ellipses, the parameter  $k$  affects only the scale but not the shape of the profile. We thus have the possibility of being able to analyze interferograms obtained by slit scanning along the axis of symmetry of the laser flare. However, we emphasize once again that the value of  $k$  must be determined.

### X-ray studies

To investigate the plasma x rays for energies  $h\nu \sim 3-10$  keV, we used multichannel detectors with a photographic film as the recording element 23, multichannel pinhole cameras 24, and multichannel scintillation counters with glass-fiber light guides 25. For energies  $h\nu > 50$  keV, the scintillation counters for hard x rays were the neutron counters 26<sup>[11]</sup> with aluminum filters of between 0.5 and 1.5 cm and lead filters of between 0.55 and 5 mm.

We used four multichannel film detectors, each incorporating 14 detection channels with beryllium filters of between 200 and 2400  $\mu$ , which enabled us to vary the long-wave limit of the spectral band (corresponding to the attenuation of intensity by a factor of  $e$ ) between 3 and 7.5 keV. The availability of several multichannel detectors enabled us to investigate the directionality of the x-ray plasma emission<sup>[8]</sup> and to analyze the spectral composition of the radiation in a sufficiently broad range. This was essential for measurements of the electron "temperature"  $T_e$  by the filter method.<sup>[14]</sup>

To investigate the spatially resolved plasma luminosity in the band between 3 and 10 keV, we used an 18-channel detection system 24 (pinhole cameras), which enabled us to carry out measurements in directions both perpendicular and parallel to the surface of the target (Fig. 3). The filters were 300–1100  $\mu$  beryllium foils. The spatial resolution of the system over the object was up to 20  $\mu$ .

Let us now consider the type of information that can be obtained when the laser flare is recorded by a pinhole camera. The first step is to determine the luminosity of the laser plasma throughout its volume. For this purpose, the number of x rays recorded at each point on the film was converted into the surface luminance of the plasma, using the data on the absolute sensitivity of the photographic film obtained in<sup>[15]</sup>. A

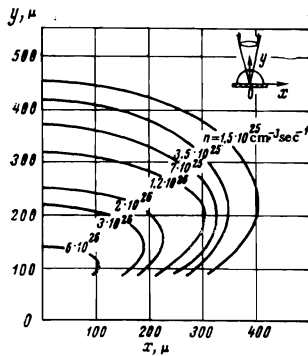


FIG. 4. Typical luminance chart obtained by analyzing pinhole camera photographs. Target—Al, filters—beryllium foil, flux density— $3 \times 10^{14}$  W/cm<sup>2</sup>.

well-defined axial symmetry of the luminous part of the flare (see Fig. 3a) was established in most cases (~90%). This enabled us to use the Abel transformation to determine the volume luminance of the flare from its surface luminance. Figure 4 shows the characteristic features of the flare luminance distribution obtained by a computerized method similar to that employed in the analysis of interferograms.

The second step in the processing of the pinhole-camera photographs enables us to determine both the electron temperature and the density profiles for the plasma. Comparison of the luminance charts obtained in different spectral regions, based on the assumption of a Maxwell distribution of electron velocities, can be used to determine the electron-temperature distribution. Using the expression relating the luminance of the plasma to its density and temperature,<sup>[16]</sup> it can be shown that the plasma-density profile is given by

$$N_e = n^{3/2} \frac{bT_e^{3/2}}{Z^{3/2} \exp(6.8 \cdot 10^{-3} Z^2 / T_e)} J^{1/2},$$

where  $n$  is the number of photons emitted per unit volume while the plasma is at temperature  $T_e$ ,  $b$  is a coefficient representing the emissive power, the magnification of the pinhole camera, and the sensitivity of the photographic film, and  $J$  is an integral which takes into account the spectral distribution of the radiation and the transmission of the filters.<sup>[15]</sup>

The correct determination of plasma parameters from the photographs obtained with the pinhole cameras is subject to considerable difficulties. They include, above all, the fact that the electron-velocity distribution is not Maxwellian and, therefore, there is some uncertainty in the very idea of "temperature."

#### Investigation of reflected and scattered radiation

The spectral composition of light reflected and scattered in different directions was investigated at frequencies  $\omega_0$ ,  $\frac{3}{2}\omega_0$ , and  $2\omega_0$  with the aid of the VMS-1 and MDR-2 monochromators (28), used as spectrographs, and the ISP-51 prism spectrograph. The energy of the incident and reflected radiation was determined with the aid of the calorimeters (29), and the shape of the pulses at the fundamental and harmonic

frequencies was determined with the EOC, used as a photorecorder, and the coaxial photocells (30).

Moreover, we investigated the space and time dependence of plasma emission at the frequency of the harmonics of the heating radiation. For this purpose, the image of the plasma in the direction perpendicular to the laser beam was passed through interference filters, or taken from the exit slit of the ISP-51 spectrograph (producing spatial resolution), onto the electron slit of the photorecorder in which the image was time-scanned. The photorecorder slit was at right-angles to the surface of the target. As in the case of the interferograms, the spatial resolution on the object was ~50 lines/mm for a time resolution of  $10^{-10}$  sec.

## 2. DISCUSSION OF EXPERIMENTAL RESULTS

The shape of the electron-density profile and its evolution during the laser pulse are important for the understanding of the processes occurring when high-power radiation interacts with the plasma corona.

For electron densities in the range  $N_e \sim 10^{18} - 2 \times 10^{19}$  cm<sup>-3</sup>, the plasma profile was determined in the course of the analysis of the interferograms. It was found that, toward the end of the laser pulse (after 2–3 nsec), the density profile was perturbed, shifting toward lower densities (Fig. 5) and, in some flares, the plasma density increased discontinuously by a factor of 2–3. The velocity of this density jump at this time was  $\sim 5 \times 10^7$  cm/sec.

It is important to note that, although the critical plasma density of the probing radiation is  $4 \times 10^{21}$  cm<sup>-3</sup>, measurements of the density profile in the range  $> 5 \times 10^{18}$  cm<sup>-3</sup> are impossible during the first two nanoseconds because of the formation of the "opacity" zone which propagates to a distance of about 1 mm from the surface of the target during the first nanosecond (see Fig. 2a). This "opacity" zone has previously been observed in laser plasma (see, for example,<sup>[17]</sup>). Its appearance is due to the refraction of the probing radia-

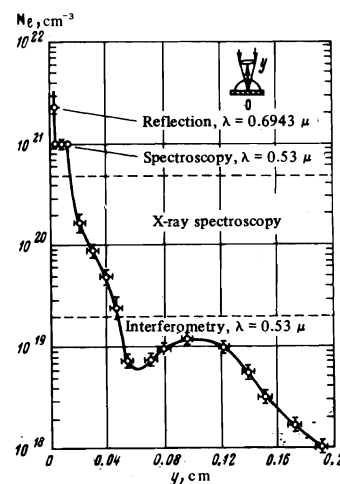


FIG. 5. Electron-density profile for laser plasma after 2 nsec, obtained for given flare by different methods. Target—Al, flux density— $3 \times 10^{14}$  W/cm<sup>2</sup>.

tion by the high density gradient, leading to a high density of interference bands which cannot be resolved by the equipment. Another consequence of this refraction phenomenon is the deviation of the rays out of the effective aperture of the objective. Experimental tests have shown, however, that, in our case, the refraction angle was smaller than the angle of view of the optical system. The spatially unresolved character of the opacity zone can also be explained<sup>[18]</sup> by the spreading of the interference bands through insufficient time resolution. It is important to remember, however, that the rate of displacement of the interference bands can be smaller than the rate of expansion of the plasma.

The increasing amount of information on the processes occurring in the plasma corona has led to other possible explanations of the opacity zone when laser plasma is investigated by optical methods resulting in the visualization of inhomogeneities. Thus, an alternative explanation can be based on depolarization (rotation of the plane of polarization) of the object ray in the region of spontaneous local magnetic fields, which apparently can reach values as high as  $\sim 10^6$  gauss.<sup>[19]</sup> The angle of rotation of the plane of polarization per unit path length in the plasma is given by<sup>[20]</sup>

$$\varphi \approx \frac{1}{2} \frac{\Omega}{c} \frac{\omega_p^2}{\omega_0^2} \cos \theta,$$

where  $\Omega = eB/mc$  is the electron gyroscopic frequency and  $\theta$  is the angle between the direction of propagation of the light wave and the magnetic field vector  $\mathbf{B}$ .

Another possible explanation can be based on the fact that the flux densities reached in the experiment exceed by not less than an order of magnitude the threshold value necessary for the development of parametric potential instabilities which can develop at points on the profile with critical density  $N_{e \text{ crit}}$  and at one-quarter of the critical density  $N_{e \text{ crit}}/4$ .<sup>[4, 7]</sup> As a result, the plasma enters a turbulent state with a high level of plasma oscillations. It is clear that, when the object ray passes through this turbulent plasma, its coherence is reduced (see<sup>[21]</sup>). The result is that interferometric measurements may become impossible in the turbulent region of the laser plasma because of the loss of coherence in the object ray.

This may also occur in interferometric studies of plasmas produced by  $\text{CO}_2$  laser radiation for which the critical density is lower by a factor of two as compared with our experiment. However, it is interesting to note that the maximum density measured interferometrically for  $\text{CO}_2$  plasma is also reduced (roughly by an order of magnitude).<sup>[22]</sup> In this respect, a reduction in the wavelength of the probing beam (for example, transition to the x-ray region) under the conditions of developed turbulence may again prevent us from examining higher densities because the degree of coherence  $\gamma$  is an exponentially decreasing function of wavelength  $\lambda$ , i. e.,  $\gamma \sim \exp(-4\pi^2/\lambda^2)$ .<sup>[21]</sup>

The size of the opacity zone is sharply reduced on the trailing edge of the laser pulse, and the range of measured densities expands up to  $\sim 5 \times 10^{19} \text{ cm}^{-3}$ . After a

few nanoseconds following the end of the laser pulse, the size of the opacity zone again increases but, this time, this is connected with the discharge of the target material.

The electron-density profile in the range  $10^{19}$ – $10^{20} \text{ cm}^{-3}$  was determined from the photographs obtained with the x-ray pinhole cameras (Fig. 5). Initially, luminance diagrams were used to determine the electron-temperature distribution within the volume of the plasma. It was found that, in the direction of the laser beam,  $T_e$  fell from about 1 keV at a distance of about 100  $\mu$ , down to 0.2 keV at a distance of about 400  $\mu$ . The electron-density profile was determined from known temperature and luminance, bearing in mind the fact that the main contribution to the x-ray emission is due to recombinations to the ground state. It is important to note that the use of the x-ray spectroscopy method in the case of plasmas with the critical ( $N_{e \text{ crit}}$ ) and quarter critical ( $N_{e \text{ crit}}/4$ ) densities requires the simultaneous use of the spatial distribution and spectral composition of the plasma x rays. The point is that the development of parametric potential instabilities in these plasma regions leads to a distortion of the electron distribution function in the region of epithermal velocities ( $V \gg V_{Te}$ ) which, in this region, becomes close to the distribution function for an electron beam propagating in the direction of the electric field vector  $\mathbf{E}$ . The slowing down of these fast electrons by plasma ions may lead to an anisotropy in the x-ray emission<sup>[23]</sup> and, consequently, in the "temperature" measured by the filter method. The pinhole camera photographs were not, therefore, analyzed for plasma regions with  $N_e > 10^{20} \text{ cm}^{-3}$ . Another reason for this was the inadequate spatial resolution for these regions.

The well-defined hemispherical shape of the flare was disturbed in about 10% of all flares. We observed the formation of either radial "jets" of enhanced luminance, or the flare image was confined to the direction perpendicular to the target surface (Figs. 3c and d). This rare appearance of luminous "jets" was noted in a series of pulses for which most of the photographs indicated a spherical shape under constant conditions. At first sight, it is natural to associate these jets with cumulative effects due to the formation of a conical crater<sup>[24]</sup> on the target, but this is characteristic only for sufficiently long laser pulses ( $\tau \sim 10^{-8}$  sec). However, the appearance of such jets was found to take place even when the target was in the form of a foil of thickness much less than the diameter of the focal spot (for example, a 10- $\mu$  aluminum foil). It follows that this effect must be due to some other factor, for example, the self-focusing of the heating radiation in the plasma. It is also important to note that, in some experiments in which scintillation x-ray counters based on the neutron counters were used, we recorded hard x rays with energies in excess of 150 keV.

To determine the dynamics of the critical-density point in the plasma profile ( $N_{e \text{ crit}} = 10^{21} \text{ cm}^{-3}$ ) with the aid of the EOC used as a photorecorder, we observed the space-time evolution of the plasma radiation at the wavelength of the second harmonic of the probing-ra-

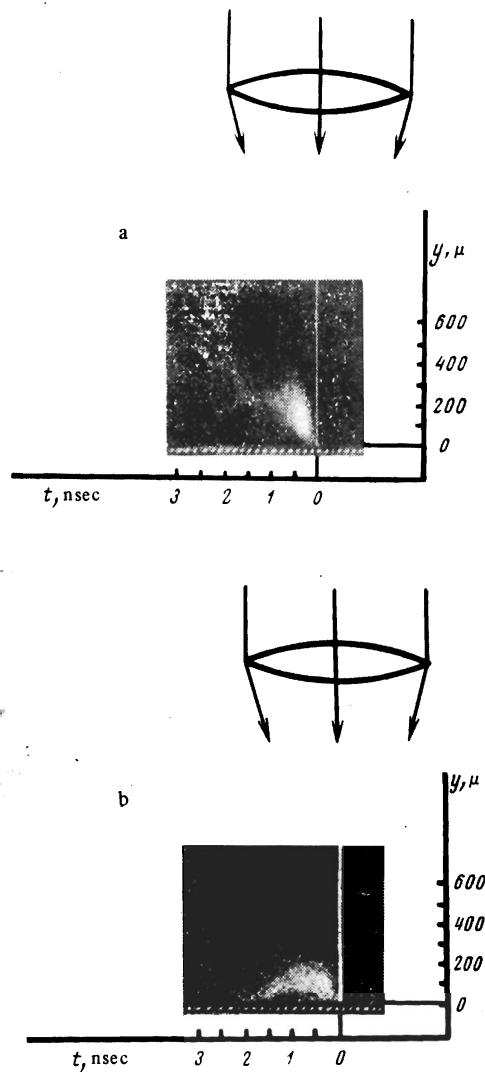


FIG. 6. Typical time scan photographs of the luminous part of the plasma at second-harmonic frequency.

radiation frequency. The point is that, according to theoretical predictions, second-harmonic generation occurs in the plasma region with  $N_e \sim N_{e \text{ crit}}$  due to the coalescence ( $l + t_0 - t_{2\omega}$ ) of a Langmuir electron oscillation  $l$  with a transverse light wave  $t_0$ , or the coalescence of two Langmuir oscillations ( $l + l - t_{2\omega}$ ), independently of the mechanism used to excite these oscillations.<sup>[7]</sup> The region in which the plasma radiates at the second-harmonic frequency can probably be identified with the region in which  $N_e \approx N_{e \text{ crit}}$ .

Figure 6a shows time-scan photographs of the plasma emission zone at the second-harmonic frequency. Initially, the radiating region moves with a velocity of about  $5 \times 10^7$  cm/sec, slowing down at the end of the laser pulse, although in some flares the bright zone moves back slightly toward the target at the end of the pulse (Fig. 6b). It is interesting to note that the bright region expands in the course of time in the direction of the heating beam to a distance of about  $100 \mu$ , and occasionally even up to  $200 \mu$ . Estimates show that the observed expansion is not related to the geometry of

the experiment and is undoubtedly a physical phenomenon.

We may thus suppose that a singularity with a linear size of  $100\text{--}200 \mu$  is present on the density profile in the critical region. The fact that the gradient changes sharply in the region of  $N_{e \text{ crit}}$  appears to be supported by the results reported in<sup>[6]</sup>, where the reflection of the probing ruby-laser radiation (the plasma was produced by a neodymium laser) was used to estimate the electron-density gradient at the point with  $N_e \sim 2.4 \times 10^{21} \text{ cm}^{-3}$ . Estimates showed that the density gradient increased sharply for  $N_e > 10^{21} \text{ cm}^{-3}$ .

Another possible reason for the expansion of the observed plasma luminance zone at the second-harmonic frequency is that the point on the profile at which the density is  $N_{e \text{ crit}}$  may execute oscillations in space in the direction of the laser beam with a period smaller than the time resolution of the photorecorder (i. e., less than  $10^{-10}$  sec). A possible explanation of the presence of the singularity at the point with density  $N_{e \text{ crit}}$  is a sharp increase in the light pressure  $P_l \approx q/c$ , which may reach  $P_l \approx 3 \times 10^5$  atm for  $q \sim 10^{15} \text{ W/cm}^2$ . This is comparable with the thermal pressure. It is also important to remember that, under the conditions of our experiment, a substantial proportion of the laser radiation is  $p$ -polarized, i. e., it has an electric-field component perpendicular to the plasma surface. This may lead to a sharp increase in the longitudinal component of the electric field<sup>[25]</sup> in the region of the critical point. If the light pressure is substantially greater than the thermal pressure,<sup>[26]</sup> plasma may become accelerated and, in the case of ions of one type,  $V = (E^2/4\pi m_i m_i)^{1/2}$ . All this can produce a distortion of the density profile in the region of the critical point, and the formation of fast ions which, under conditions close to those prevailing in our experiment, may reach an appreciable fraction of a percent of the total number of ions in the corona, with characteristic acceleration time  $\sim 10^{-11}$  sec.<sup>[27]</sup> Model experiments in the microwave region<sup>[28]</sup> have demonstrated the formation of a perturbation (caviton) on the density profile in the region of the critical point, and its propagation toward lower densities.

Measurements of the energy and spectral composition of the reflected and scattered radiation showed that the fraction of energy reflected from the plasma at the fundamental frequency into the solid angle of the focusing system was low (less than 0.5–1%), as in the case of lower flux densities.<sup>[7]</sup> It is important to remember, however, that the target was at a small angle to the laser beam and, in the case of "specular" reflection<sup>[8]</sup> from the flat target, this may lead to a reduction in the coefficient of reflection into the solid angle of the focusing system.

Measurements of the spectral composition of the incident and back-reflected radiation show that the intensity maxima of lines corresponding to both the incident and reflected radiation approximately correspond to  $\lambda_0 = 10\,600 \text{ \AA}$ , and the width of their spectra is about  $50 \text{ \AA}$  at half-intensity points.

The line shapes were found to be similar and, in con-

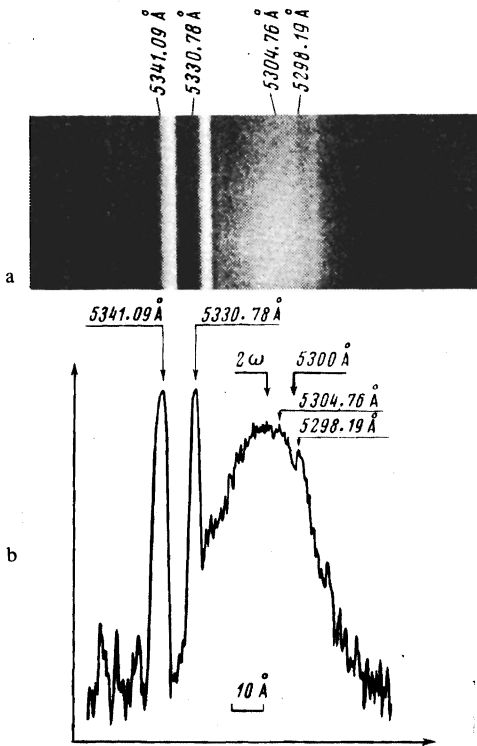


FIG. 7. (a) Typical spectrogram of second-harmonic line in light reflected from plasma for a shift of  $\sim 8.3$  Å. (b) Densitometer plot of the same photograph. The following neon lines were used as standards: 5341.09 Å, 5330.78 Å, 5304.76 Å, 5298.19 Å.

trast to<sup>[29,30]</sup>, no appreciable shifts were recorded for the maximum of the reflected line. These features do not enable us to elucidate unambiguously the origin of the reflected radiation. Possible mechanisms include ordinary reflection from the plasma region with critical density and stimulated Mandel'shtam-Brillouin scattering (SMBS).<sup>[31]</sup>

Measurements on the spectrum of radiation scattered by plasma into the aperture of the focusing system at the second-harmonic frequency showed that the intensity maximum of the second-harmonic line was shifted relative to the wavelength  $\lambda_{2\omega_0} = \lambda_0/2 = 5300$  Å toward longer wavelengths by an amount ranging from  $\Delta\lambda \approx 2.5$  Å to  $\Delta\lambda \approx 8$  Å. Spectrograms of the second harmonic showed that it was always asymmetrically red-shifted (Fig. 7).

The degree of asymmetry, i.e., the ratio of the red half-width to the blue half-width was found to vary between 1.06 and 1.65 at half-intensity points, and between 1.16 and 1.41 at the points corresponding to one-tenth of the intensity maximum. As a rule, the greater the shift, the greater the degree of asymmetry. Red shifts of second-harmonic lines were previously reported in<sup>[32,33]</sup> for picosecond laser pulses, and the asymmetric broadening of the spectrum was observed in<sup>[33,36]</sup>. Symmetric broadening was reported in<sup>[32]</sup>.

Possible reasons for the generation of the second harmonic in the plasma include linear transformation of the laser radiation by the density gradient,<sup>[37,38]</sup> and

development of parametric instabilities in the neighborhood of the critical density, i.e., aperiodic instability of the form  $t_0 - l_a + a$ , parametric decay of the incident light wave into Langmuir electron and ion-acoustic oscillations  $t_0 - l_s + s$ , and SMBS of the form  $t_0 - t_s + s$ . The second harmonic can be generated through the coalescence of a transverse light wave with a Langmuir electron potential oscillation, or the coalescence of two Langmuir oscillations, but the probability of the second process is much smaller.<sup>[38]</sup> The coalescence of a transverse light wave with a Langmuir wave  $l_a$  generated by an aperiodic instability leads to a shift of the second-harmonic line peak toward shorter wavelengths. This is due to the fact that the frequency of the resulting Langmuir electron oscillation  $l_a$  is greater than  $\omega_0$ . The process  $t_0 + l_a - t_{2\omega}$  can therefore be rejected because it is inconsistent with the present experimental data. The remaining two most probable processes involving coalescence, namely,  $t_0 + l_s - t_{2\omega}$  and  $t_s + l_s - t_{2\omega}$  (remembering that the shift of  $t_2$  is largely determined by the shift of the frequency of  $l_s$  relative to  $\omega_0$ ), the magnitude of the red shift  $\Delta\lambda_{2\omega}$  of the second-harmonic line is given by the single expression (in ångströms)<sup>[39]</sup>

$$\Delta\lambda_{2\omega} = (Z/A)^{1/2} [20T_e + 7 \cdot 10^{-13} q (a/\lambda_0)^{3/2}]^{1/2},$$

where  $T_e$  is the electron temperature in keV,  $q$  is the flux density of the laser radiation on the target in  $W/cm^2$ ,  $a$  is a characteristic linear dimension of the plasma inhomogeneity,  $A$  is the mass number, and  $Z$  the atomic number of the target material. This expression is obtained by analyzing the dispersion relation for the disturbed plasma which is parametrically unstable in the presence of a high-power pump field. When the flux density  $q$  is not too high, and the first term in the brackets is not small in comparison with the second, the electron plasma temperature  $T_e$  in the neighborhood of the critical point can be determined if  $\Delta\lambda_{2\omega}$  is known (at high flux densities  $q$ , the shift  $\Delta\lambda_{2\omega}$  no longer depends on  $T_e$ ). In the experiment with the aluminum target ( $Z = 13$ ,  $A = 27$ ), the light flux density  $q = 2 \times 10^{14}$   $W/cm^2$  corresponded to a shift  $\Delta\lambda_{2\omega} \approx 5$  Å, which yielded  $T_e \approx 1$  keV ( $a \sim 10^{-2}$  cm). This estimate is close to that obtained from the analysis of the pinhole camera photographs for a density  $N_e \approx 10^{20}$   $cm^{-3}$ . We emphasize once again that estimates of the electron temperature in the plasma deduced from the shift of the second-harmonic line characterize the local temperature in the neighborhood of the critical-density point.

In conclusion, we should like to express our gratitude to Academician N. G. Basov for his constant interest in this work, to V. P. Silin for stimulating discussions, to V. V. Pustovalov for useful suggestions, and to A. A. Eorkhin and A. A. Kologrivov for assistance in this research.

<sup>1</sup>N. G. Basov, E. G. Gamaly, O. N. Krokhin, Yu. A. Mikhailov, G. V. Sklizkov, and S. I. Fedotov, *Laser Interaction and Related Plasma Phenomena*, 3, Plenum Press, 1974.

<sup>2</sup>N. G. Basov, Yu. A. Zakharenkov, O. N. Krokhin, Yu. A. Mikhailov, G. V. Sklizkov, and S. I. Fedotov, *Kvantovaya Elektron. (Moscow)* 1, 2069 (1974); [*Sov. J. Quantum Elec-*

- tron. 4, 1154 (1975)]. P. M. Cambell, G. Charatis, and G. R. Montry, Phys. Rev. Lett. 34, 74 (1975).
- <sup>3</sup>J. Nuckolls, L. Wood, A. Thiessen, and G. Zimmerman, Nature 239, 139 (1972); Yu. V. Afanas'ev, N. G. Basov, P. P. Volosevich, E. G. Gamaliĭ, O. N. Krokhin, S. P. Kurdyumov, B. I. Levanov, V. B. Rozanov, A. N. Tikhonov, and A. A. Samarskiĭ, Pis'ma Zh. Eksp. Teor. Fiz. 21, 150 (1975) [JETP Lett. 21, 68 (1975)].
- <sup>4</sup>V. P. Silin, Parametricheskoe vozeĭstvie izlucheniya bol'shoĭ moshchnosti na plazmu (Parametric Interaction Between High-Power Radiation and Plasma), Nauka, 1973.
- <sup>5</sup>A. A. Rupasov, V. P. Tsapenko, and A. S. Shikanov, Preprint No. 94, FIAN SSSR, 1972.
- <sup>6</sup>A. A. Rupasov, G. V. Sklizkov, V. P. Tsapenko, and A. S. Shikanov, Zh. Eksp. Teor. Fiz. 65, 1898 (1973) [Sov. Phys. JETP 38, 947 (1974)]; Preprint No. 53, FIAN SSSR, 1973.
- <sup>7</sup>N. G. Basov, O. N. Krokhin, V. V. Pustovalov, A. A. Rupasov, V. P. Silin, G. V. Sklizkov, V. T. Tikhonchuk, and A. S. Shikanov, Zh. Eksp. Teor. Fiz. 69, 206 (1975) [Sov. Phys. JETP 42, 107 (1976)]; Preprint No. 17, FIAN SSSR, 1974.
- <sup>8</sup>O. N. Krokhin, Yu. A. Mikhaĭlov, V. V. Pustovalov, V. P. Silin, G. V. Sklizkov, and A. S. Shikanov, Zh. Eksp. Teor. Fiz. 69, 206 (1975) [Sov. Phys. JETP Preprint No. 22, FIAN SSSR, 1975].
- <sup>9</sup>N. G. Basov, O. N. Krokhin, G. V. Sklizkov, S. I. Fedotov, and A. S. Shikanov, Zh. Eksp. Teor. Fiz. 62, 203 (1972) [Sov. Phys. JETP 35, 109 (1972)].
- <sup>10</sup>N. G. Basov, O. N. Krokhin, G. V. Sklizkov, and S. I. Fedotov, Tr. Fiz. Inst. Akad. Nauk SSSR 76, 146 (1974).
- <sup>11</sup>V. M. Groznov, A. A. Erokhin, Yu. A. Zakharenkov, N. N. Zorev, N. A. Konoplev, O. N. Krokhin, G. V. Sklizkov, S. I. Fedotov, and A. S. Shikanov, "Vysokoskorostnaya interferometriya nestatsionarnoi plotnoi lazernoĭ plazmy" (High-Speed Interferometry of Nonstationary Dense Laser Plasma), Preprint No. 50, FIAN SSSR, 1975.
- <sup>12</sup>H. Ertel, in: Physics of Fast Processes (Russ. Transl., Mir, 1971, p. 103).
- <sup>13</sup>Yu. A. Zakharenkov, N. N. Zorev, A. A. Kologrivov, N. A. Konoplev, G. V. Sklizkov, and S. I. Fedotov, Preprint No. 121, FIAN SSSR, 1973.
- <sup>14</sup>F. C. Jahoda, E. M. Little, W. E. Quinn, G. A. Sawyer, and T. F. Stratton, Phys. Rev. 119, 843 (1960).
- <sup>15</sup>A. A. Kologrivov, Yu. A. Mikhaĭlov, G. V. Sklizkov, S. I. Fedotov, A. S. Shikanov, and M. R. Shpol'skiĭ, Preprint No. 46, FIAN SSSR, 1975; Kvantovaya Elektron. (Moscow) No. 10, 2223 (1975) [Sov. J. Quantum Electron. 5, 1210 (1975)].
- <sup>16</sup>I. I. Sobel'man, Vvedenie v teoriyu atomnykh spektrov (Introduction to the Theory of Atomic Spectra), Fizmatgiz, 1963 [Plenum, 1966].
- <sup>17</sup>N. G. Basov, O. N. Krokhin, and G. V. Sklizkov, Laser Interaction and Related Plasma Phenomena, 2, Plenum Press, 1972.
- <sup>18</sup>G. V. Sklizkov, in: Laser Handbook, 2, North-Holland, Amsterdam, 1972, p. 1545; D. T. Attwood and L. W. Coleman, Appl. Phys. Lett. 24, 408 (1974).
- <sup>19</sup>J. A. Stamper, K. Papadopoulos, R. N. Sudan, W. A. McLean, and J. M. Dawson, Phys. Rev. Lett. 26, 1012 (1972).
- <sup>20</sup>L. D. Landau and E. M. Lifshitz, Élektrodinamika sploshnykh sred (Electrodynamics of Continuous Media), Gostekhnizdat, 1957 [Pergamon, 1968].
- <sup>21</sup>J. L. Ho, J. Opt. Soc. Am. 60, 667 (1970).
- <sup>22</sup>L. C. Johnson and T. K. Chu, Phys. Rev. Lett. 32, 517 (1974); G. Tonon and M. Rabeau, Plasma Phys. 15, 871 (1973); P. T. Rumsby and M. M. Michaelis, Phys. Lett. A 49, 413 (1974).
- <sup>23</sup>O. N. Krokhin, Yu. A. Mikhaĭlov, V. V. Pustovalov, A. A. Rupasov, V. P. Silin, G. V. Sklizkov, and A. S. Shikanov, Pis'ma Zh. Eksp. Teor. Fiz. 20, 239 (1974) [JETP Lett. 20, 105 (1974)].
- <sup>24</sup>V. A. Gribkov, O. N. Krokhin, V. Ya. Pikulin, O. G. Semenov, and G. V. Sklizkov, Kvantovaya Elektron. (Moscow) 2, 975 (1975) [Sov. J. Quantum Electron. 5, 530 (1975)].
- <sup>25</sup>N. G. Denisov, Zh. Eksp. Teor. Fiz. 31, 609 (1956) [Sov. Phys. JETP 4, 544 (1975)]. V. L. Ginzburg, Rasprostranenie elektromagnitnykh voln v plazme (Propagation of Electromagnetic Waves in Plasma), Nauka, 1967.
- <sup>26</sup>A. B. Gurevich and V. P. Silin, Yad. Fiz. 2, 250 (1965) [Sov. J. Nucl. Phys. 2, 179 (1966)].
- <sup>27</sup>V. P. Silin, Pis'ma Zh. Eksp. Teor. Fiz. 21, 333 (1975) [JETP Lett. 21, 152 (1975)].
- <sup>28</sup>A. Y. Wong, R. L. Stenzel, H. C. Kim, and F. F. Chen, Fifth Intern. Conf. on Plasma Physics and Thermonuclear Fusion, CN-33/H 4-1, Tokyo, November 11-15, 1974.
- <sup>29</sup>K. Büchl, K. Eidman, A. Zalzman, and R. Sigel, Appl. Phys. Lett. 20, 231 (1972).
- <sup>30</sup>D. Beland, C. De Michelis, M. Mattioli, and R. Popular, Appl. Phys. Lett. 21, 52 (1972).
- <sup>31</sup>L. M. Gorbunov, Zh. Eksp. Teor. Fiz. 65, 990 (1973) [Sov. Phys. JETP 38, 490 (1974)].
- <sup>32</sup>L. M. Goldman, J. Soures, and M. J. Lubin, Phys. Rev. Lett. 31, 1184 (1973).
- <sup>33</sup>P. Lee, D. V. Giovanelli, R. P. Godwin, and G. H. McCall, Appl. Phys. Lett. 24, 406 (1974).
- <sup>34</sup>J. L. Bobin, M. Decroisette, B. Meyer, and Y. Vitel, Phys. Rev. Lett. 30, 594 (1973).
- <sup>35</sup>M. Decroisette, B. Meyer, and Y. Vitel, Phys. Lett. A 45, 443 (1974).
- <sup>36</sup>A. A. Gorokhov, V. D. Dyatlov, R. N. Medvedev, A. D. Starikov, and V. G. Tuzov, Pis'ma Zh. Eksp. Teor. Fiz. 21, 111 (1975) [JETP Lett. 21, 49 (1975)].
- <sup>37</sup>N. S. Erokhin, S. S. Moiseev, and V. V. Mukhin, Nucl. Fuz. 14, 333 (1975).
- <sup>38</sup>A. V. Vinogradov and V. V. Pustovalov, Zh. Eksp. Teor. Fiz. 63, 940 (1972) [Sov. Phys. JETP 36, 492 (1973)].
- <sup>39</sup>O. N. Krokhin, V. V. Pustovalov, A. A. Rupasov, V. P. Silin, G. V. Sklizkov, A. N. Starodub, V. T. Tikhonchuk, and A. S. Shikanov, Pis'ma Zh. Eksp. Teor. Fiz. 22, 47 (1975) [JETP Lett. 22, 21 (1975)].

Translated by S. Chomet